



ELSEVIER

16 June 1994

PHYSICS LETTERS B

Physics Letters B 329 (1994) 332-337

Spin dependence of the heavy-quark potential: a QCD lattice analysis

K.D. Born^a, E. Laermann^b, T.F. Walsh^c, P.M. Zerwas^d

^a *Inst. Theor. Physik, RWTH Aachen, D-52074 Aachen, FRG*

^b *Fakultät für Physik, Universität Bielefeld, D-33501 Bielefeld, FRG*

^c *Physics Dept., University of Minnesota Minneapolis, MN 55455, USA*

^d *Deutsches Elektronen-Synchrotron DESY, D-22603 Hamburg, FRG*

Received 18 February 1994

Editor: P.V. Landshoff

Abstract

We have investigated the spin dependence of the potential between heavy quarks in full lattice QCD, including the effects of light quark loops. The form of the spin-orbit, the tensor and the spin-spin forces present clear evidence for long-range scalar confinement supplemented by a Coulomb force at short distances. This agrees with observations from quarkonium spectroscopy. The QCD simulation has been carried out for Kogut-Susskind fermions with four degrees of freedom at a gauge coupling $\beta = 5.35$ and a quark mass $am_q = 0.01$ on a $16^3 \times 24$ size lattice. This corresponds to a lattice spacing 0.12 fm, a spatial lattice size of about 2 fm and a light quark mass of 48 MeV.

1. Basis

The interquark forces in heavy quarkonia present a very interesting opportunity to study the strong interactions in a simple situation. The spectroscopy of charmonium and bottonium states is sensitive to interquark distances between 0.1 and 1 fm [1]. The toponium ground state (accessible if the top mass is not heavier than ~ 180 GeV) will probe distances down to ~ 0.01 fm [2,3]. The rich spectroscopy of charmonium and bottonium states is well described by potential models that incorporate a spin-independent static potential at large distances and spin-dependent forces which induce the fine- and hyperfine-splitting of the energy levels. From the analysis of experimental data, a de-

tailed picture of confining and spin-dependent forces emerged some time ago. As a next step, we need to show that QCD can properly account for these forces. While perturbation theory provides an adequate instrument to tackle this problem at short distances, the long-distance behavior can only be studied in the lattice formulation of QCD at present.

In a preceding note [4], we have described our results for the static confinement potential in a QCD simulation that includes quark loops. Here we concentrate on the spin-dependent forces. The most general form of the interquark $q\bar{q}$ potential up to order v^2/c^2 of the expansion in the quark velocity may be written [5]

Table 1

Contributions of the scalar and vector parts of the static potential to the spin-dependent terms V_i

V_{stat}	δV_1	δV_2	δV_3	δV_4
V_S	$-V_S$	0	0	0
V_V	0	V_V	$-(V_V' - V_V'/r)$	$2\Delta V_V$
$V_V = -\frac{e}{r}$	0	$-\frac{e}{r}$	$\frac{3e}{r^3}$	$-8\pi e\delta_3(r)$

In the last row, the δV_i are shown for a Coulombic vector potential.

$$\begin{aligned}
 V_{\text{eff}}(r) &= V_{\text{stat}}(r) \\
 &+ \left(\frac{l_1 s_1}{2m_1^2} - \frac{l_2 s_2}{2m_2^2} \right) \left(\frac{V'_{\text{stat}}(r)}{r} + \frac{2V'_1(r)}{r} \right) \\
 &+ \left(\frac{l_1 s_2}{m_1 m_2} - \frac{l_2 s_1}{m_1 m_2} \right) \frac{V'_2(r)}{r} \\
 &+ \frac{1}{m_1 m_2} \left(\frac{(rs_1)(rs_2)}{r^2} - \frac{s_1 s_2}{3} \right) V_3(r) \\
 &+ \frac{s_1 s_2}{3m_1 m_2} V_4(r) \tag{1}
 \end{aligned}$$

This is a generalization of the well-known QED Breit–Fermi interaction. $m_{1,2} = m$ denote the quark/antiquark masses, $s_{1,2}$ and $l_1 = -l_2 = l$ are the spins and orbital angular momenta, and $r = r_1 - r_2$ is the distance vector between quark and antiquark.

The potentials V_i and V_{stat} are not independent of each other. As a result of Lorentz invariance the spin-orbit potentials V_1 and V_2 are related to the static potential by the Gromes relation [6]

$$V_2 - V_1 = V_{\text{stat}} \tag{2}$$

As a consequence, the spin-orbit forces cannot be built-up entirely by short-distance one-gluon exchange. They are intimately related to the confinement mechanism.

Interpreted as the static limit of a relativistically invariant interaction density, the static potential can only be built-up by scalar and vector contributions [7],

$$V_{\text{stat}} = V_S + V_V \tag{3}$$

These two components contribute quite differently to the spin-dependent parts of the interquark potential, as shown in Table 1. The observed fine-splitting of the triplet P charmonium as well as bottomonium states favors a scalar long-range confining part σr of the static potential. The spin-orbit potential V_1 is then attributed

to the confining part of the potential [1,8]. The vector one-gluon exchange contribution to the quark interactions builds up the spin-orbit potential V_2 as well as the tensor force V_3 and the spin-spin interaction V_4 .

Calculations of the spin-dependent potentials and evidence for scalar confinement have been reported from several lattice simulations. The first calculations [9,10] were done in the quenched approximation neglecting quark-loop effects. This valence-quark approach is a physically appealing first step, but it is nevertheless important to extend the calculation to full QCD including light quark degrees of freedom. Only one attempt in this direction has been reported so far, Ref. [11]. Here we report results of a full QCD simulation which substantially improves the earlier calculation in three respects. We have used a small lattice quark mass $am_q = 0.01$, corresponding to a physical light quark mass of $m_q^{\text{RGI}} = 48$ MeV. Our lattice spacing is 0.12 fm, leading to an overall lattice size of 1.9 fm. We have been able to determine the spin-dependent potential off axis on the lattice diagonals for the first time, a necessary step in demonstrating rotational invariance. The statistical significance has been improved as well.

2. Technique

The spin-dependent potentials V_1 to V_4 can be written as correlations between color-electric and color-magnetic fields at the positions of the quark and antiquark in the color dipole, averaged over time [5]:

$$\begin{aligned}
 \frac{r_k}{r} V'_1(r) &= \frac{\epsilon_{ijk}}{2T} \int \int dt dt' (t' - t) \\
 &\times \langle g_s^2 B_i(\mathbf{r}_1, t) E_j(\mathbf{r}_1, t') \rangle_W / \langle 1 \rangle_W \tag{4}
 \end{aligned}$$

$$\begin{aligned}
 \frac{r_k}{r} V'_2(r) &= \frac{\epsilon_{ijk}}{2T} \int \int dt dt' (t' - t) \\
 &\times \langle g_s^2 B_i(\mathbf{r}_2, t) E_j(\mathbf{r}_1, t') \rangle_W / \langle 1 \rangle_W \tag{5}
 \end{aligned}$$

$$\begin{aligned}
 \left(\frac{r_i r_j}{r^2} - \frac{\delta_{ij}}{3} \right) V_3(r) + \frac{\delta_{ij}}{3} V_4(r) &= \frac{1}{T} \int \int dt dt' \\
 &\times \langle g_s^2 B_i(\mathbf{r}_1, t) B_j(\mathbf{r}_2, t') \rangle_W / \langle 1 \rangle_W \tag{6}
 \end{aligned}$$

The symbol $\langle \rangle_W$ denotes the expectation values of Wilson loops with electric and magnetic color fields inserted at the quark positions $\mathbf{r}_{1,2}$ at times t and t' .

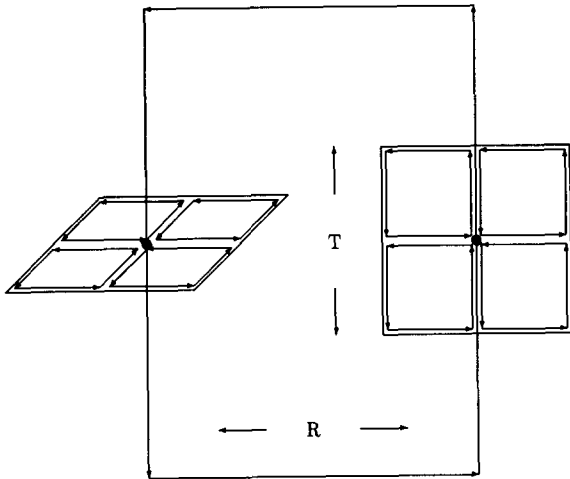


Fig. 1. Definition of the color-electric and magnetic fields on the lattice by cloverleaf arrangement of plaquettes.

$\langle 1 \rangle_W$ represents the expectation value of the Wilson loop itself. The integration runs over the time coordinates of the gluon field operators, $0 \leq t, t' \leq T$. Taking the temporal extent of the Wilson loop $T \rightarrow \infty$ projects out the dipole ground state.

The correlation functions (4)–(6) can be evaluated numerically on the lattice. Following Refs. [9,10], we define the color field strength tensor on the lattice by a suitable average over the four plaquettes touching the space-time point x [see Fig. 1]:

$$\hat{F}^{\mu\nu}(x) = \frac{1}{4} \sum_1^4 \frac{i}{2} [U_{\square}(x; \mu\nu) - U_{\square}^{\dagger}(x; \mu\nu)] \quad (7)$$

The color-electric and magnetic fields read

$$E_i(x) = \frac{1}{g_s a^2} \hat{F}_{4i}(x) \quad (8)$$

$$B_i(x) = \frac{\epsilon_{ijk}}{g_s a^2} \hat{F}_{jk}(x) \quad (9)$$

For distances $r \leq 2a$ (a being the lattice spacing) the operators partly overlap. In these cases we calculate the correlation between the plaquettes first and average subsequently.

Quark and antiquark self-energies associated with the perimeter must be removed in order to extract the Wilson loop. For simple loops, it can be proven that this contribution corresponds to a multiplicative factor [12]. If field operators are inserted, it has been shown up to $\mathcal{O}(g_s^2)$ in the pure gauge theory [10]

that the self-energies of the $E - B$ correlations can be subtracted according to the following rule¹:

$$\begin{aligned} & \langle \langle E(x_1)B(x_2) \rangle_W / \langle 1 \rangle_W \rangle^R \\ &= \frac{\langle E(x_1)B(x_2) \rangle_W \langle 1 \rangle_W}{\langle U_{\square}(x_1) \rangle_W \langle U_{\square}(x_2) \rangle_W} \end{aligned} \quad (10)$$

For numerical calculations we can assume the factorization $\langle U_{\square} \rangle_W = \langle P \rangle \langle 1 \rangle_W$, with $P = \text{Re tr } U_{\square}$, so that finally

$$\begin{aligned} & \langle \langle E(x_1)B(x_2) \rangle_W / \langle 1 \rangle_W \rangle^R \\ &= \frac{\langle E(x_1)B(x_2) \rangle_W}{\langle P(x_1) \rangle \langle P(x_2) \rangle \langle 1 \rangle_W} \end{aligned} \quad (11)$$

The last factor $\langle 1 \rangle_W$ may be interpreted as the renormalization of the loop itself, while the first two terms account for $\mathcal{O}(g_s^2)$ corrections in (7)–(9). The $B - B$ correlations are normalized according to Eq. (11). We adopt this method in our numerical procedure; it appears superior to ad hoc numerical renormalizations of the heavy quark mass. (The method can be checked by examining the validity of the Gromes relation.)

To check for restoration of rotational invariance on the lattice, we evaluated the correlation functions not only along the three lattice axes but also along the six plane-diagonal directions. For the plane-diagonal loops we varied the space directions k in the calculation of V_1 and V_2 , Eqs. (4),(5), while in the case of $V_{3,4}$, in (6), we have restricted ourselves to the evaluation of the diagonal tensor elements $i = j$.

To determine the spin-dependent potentials Eqs. (4)–(6) we require a weighted average over all time distances. This increases the numerical effort by a factor T^2 compared to the simple Wilson loop. This increase can be partly circumvented by working in the temporal gauge, in which the gauge fields in the time directions are gauge transformed to unity. (Excepting the last time layer.) We smeared the string connections along the spatial directions according to a variant of the APE prescription [14] so as to improve the projection on the flux tube between

¹ Since Lorentz invariance is only realized in a discrete manner on the lattice, relativistic $\frac{1}{m}\gamma\mathcal{D}$ corrections can mix with the static propagator through renormalization [13]. This affects the chromo-electric insertions only, $\langle \mathbf{BE} \rangle \sim \langle \mathbf{BD}^2 \rangle \sim \langle \mathbf{BD}_{\text{bare}}^2 \rangle + \langle \mathbf{B} \rangle$. However, because of parity invariance, $\langle \mathbf{B} \rangle$ vanishes, in the continuum as well as on the lattice.

Table 2

The results for the measurement of the potentials V_i as a function of τ

V	r	$\tau = t' - t$					\sum_{τ}
		0	1	2	3	4	
V'_1	1	1453 (26)	-2116 (37)	-417 (28)	-75 (18)	-13 (10)	-3230 (189)
	2	1256 (65)	-2091 (106)	-564 (76)	-148 (51)	-21 (25)	-3753 (518)
	3	1134 (133)	-1934 (212)	-510 (160)	-136(107)	-32 (53)	-3498(1069)
	4	1066 (248)	-1861 (396)	-520 (296)	-57(202)	-30 (96)	-3193(1981)
V'_2	1	-4 (24)	12077 (39)	1805 (28)	255(18)	31 (16)	16583 (188)
	2	-42 (65)	2735 (103)	961 (79)	232(51)	36 (24)	5503(5181)
	3	45 (134)	762 (215)	478 (160)	-138(105)	1 (51)	2140(1059)
	4	114 (218)	110 (398)	1225 (304)	89(194)	18 (99)	697(1990)
V_3	1	22551 (113)	2933 (178)	35 (131)	85(87)	532 (43)	26138 (554)
	2	5763 (180)	1724 (289)	210 (213)	49(147)	-14 (72)	7733 (910)
	3	1367 (370)	967 (601)	231 (447)	78(308)	49(144)	2695(1869)
	4	252 (697)	217(1144)	16 (848)	-57(566)	8(280)	436(3538)
V_4	1	-26782 (193)	3992 (304)	2000 (222)	247(148)	-990 (73)	-21532 (941)
	2	-7398 (268)	449 (432)	834 (290)	314(220)	81(105)	-5717(1349)
	3	-1424 (556)	-216 (897)	355 (673)	181(456)	125(214)	-977(2796)
	4	-378(1046)	-184(1718)	277(1274)	98(844)	-9(418)	-197(5301)

The values are given in units of a and are multiplied by a factor of 10^5 . The last column gives the (weighted) sum over τ

the heavy quarks. To keep the computer time at a tolerable level, the loops have been evaluated for a fixed time $T = 4a$. The spatial extent has been varied from $R = 0$ to $R = 4a$. Due to limited statistics, loops beyond $T = 4a$ did not improve the signal.

The correlation functions in (4)–(6) depend on the times t and t' , or equivalently $\tau = t' - t$ and $\omega = \frac{1}{2}(t' + t)$. For sufficiently large T , the expectation values should become independent of ω . This is indeed borne out by the data if the boundary values $t, t' = 0$ and T are excluded. (They are contaminated by admixtures of unwanted excited string states.) The correlation functions fall off very fast as a function of the time difference τ , so that the integral converges [10]. We demonstrate this in Table 2 where the results for the correlations of on-axis loops are listed as functions of τ .

3. Results

To extract the spin-dependent potentials V_i , the correlations of the color-electric and magnetic fields have been evaluated over an ensemble of 84 configurations obtained by the MT_c Collaboration on a $16^3 \times 24$ lat-

tice at $\beta = 5.35$ and quark mass $am_q = 0.010$. This ensemble has been generated by means of a hybrid Monte Carlo algorithm. The lattice spacing was fixed by fitting [4] the long-range part of the confinement potential to the string tension $\sigma = 1\text{GeV}/\text{fm}$, with the result $a = 0.12\text{ fm}$. (This value agrees roughly with the value extracted from the ρ mass when extrapolated to vanishing quark mass [15]). The light quark mass in this simulation is then $m^{\text{RGI}} = 48\text{ MeV}$ in physical units, corresponding to a π mass of 350 MeV.

In addition, another set of configurations has been exploited. They were obtained earlier by means of the pseudofermion algorithm. This ensemble was generated at the same $\beta = 5.35$, but at a larger quark mass $am_q = 0.025$. No striking dependence on the (small) quark mass was visible.

Our results for the spin-dependent potentials V_i ($i = 1, \dots, 4$) for $\beta = 5.35$ and $am = 0.010$ are displayed in Fig. 2 (a)–(d). The potentials, as well as the quark–antiquark separation r , are given in units of the lattice spacing a . To correct for lattice artifacts, the distances r have been improved at tree level in the manner explained in Ref. [4].

Inspecting the figures, we can draw the following

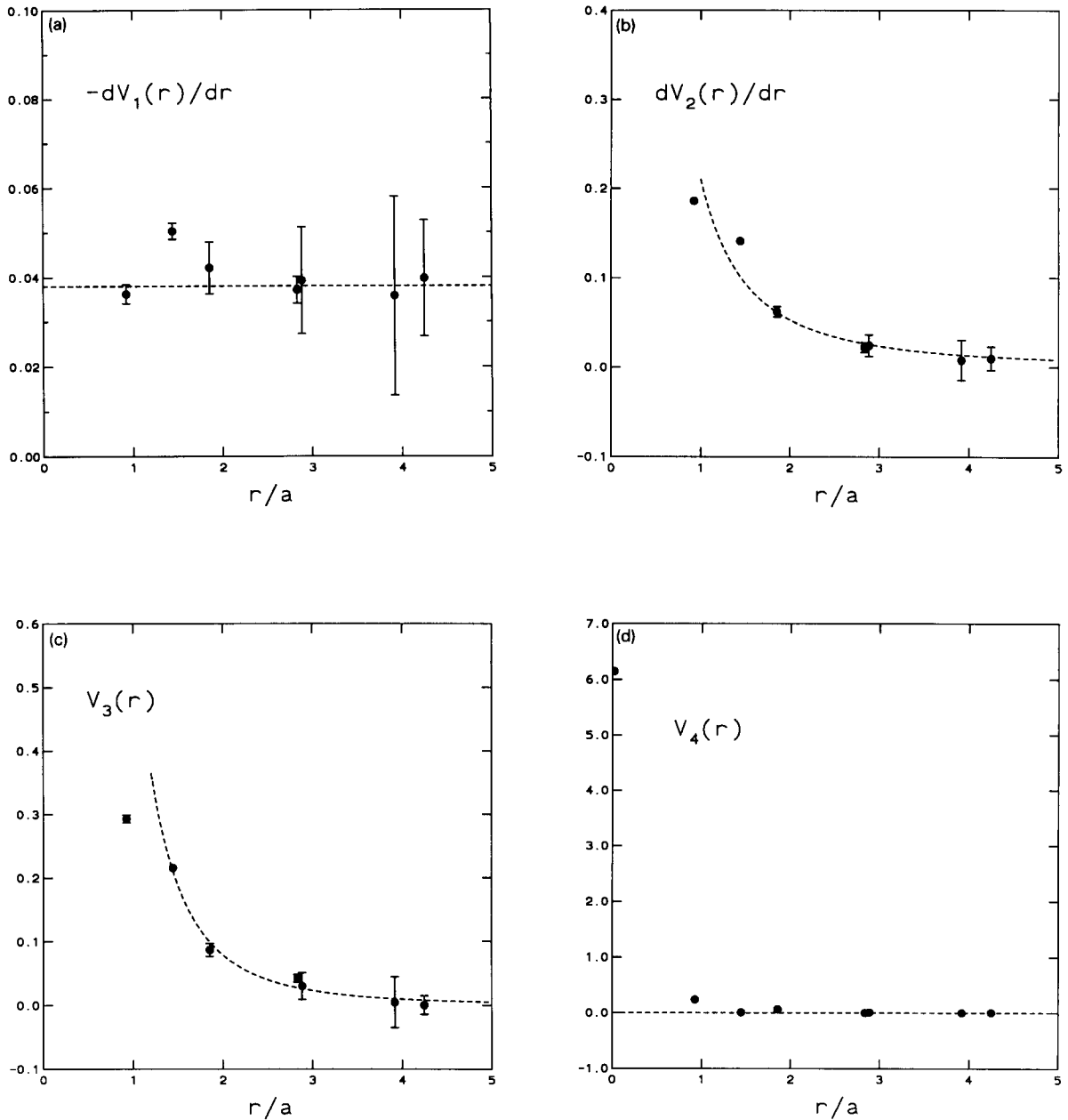


Fig. 2. The four spin-dependent interquark potentials. (a) The spin-orbit force V_1 is long range, $dV_1/dr \sim \text{const}$. The result of a fit to this form, excluding the data at small quark-anti quark separations, $r/a \leq 1.41$, is indicated by the dotted line. (b)–(d) The spin-orbit potential V_2 , the tensor force V_3 and the spin-spin force V_4 are short range. The data are compatible with expectations from one-gluon exchange, as demonstrated by dotted lines which represent results from fits to $dV_2/dr \sim 1/r^2$ (b) and $V_3 \sim 1/r^3$ (c) for $r/a > 1.41$. V_4 is compatible with a smeared $\delta_3(r)$.

conclusions.

(i) Our measurement of the potentials in the plane-diagonal directions reveals the restoration of rotational symmetry for our simulation parameters. In particular, the spatial separation $r = \sqrt{2}a$ provides precious additional information.

(ii) The derivative of the spin-orbit potential dV_1/dr is flat within the (admittedly somewhat large) error bars. This indicates that the long-range, confining part of the potential is responsible for V_1 . This is corroborated by the fact that dV_2/dr falls to zero for large r . A fit to the data which excludes the results at small distances, $r/a \leq \sqrt{2}$, returns a central value of $dV_1/dr = -0.038(3)$, about 30% smaller than the slope σ of the static potential. A (scalar) $1/r$ piece correcting the linear potential in the string picture [16] is not visible in V_1 .

(iii) The spin-orbit potential dV_2/dr and the tensor force V_3 clearly fall off quickly with r . In fact, they appear to be well described by one-gluon exchange. This is demonstrated by the dotted lines, which are fits to potentials derived from the vector Coulomb piece (see Table 1). Thus the V_2 data strongly indicate a short-range character. (Given the scatter in the data, we cannot rule out a very small constant contribution.) The couplings e extracted from the fits (for $r/a > \sqrt{2}$) come out as $e = 0.21(2)$ for both V_2 and V_3 . There is thus a nice agreement between the two potentials and with the expectation from (vector) one-gluon exchange. However, the values are approximately 20% lower than the value derived from the static potential.

(iv) The spin-spin force V_4 is zero for non-zero distances r , from $r \geq \sqrt{2}a$ onward. A large positive value is apparent at zero distance. This is compatible with a (smeared) zero range behavior $V_4(r) \sim \delta_3(\mathbf{r})$ as predicted by one-gluon exchange.

(v) With the confining part residing substantially in V_1 , and with V_2 being predominantly short-ranged, the Gromes relation (2) is satisfied only at a level of 20 to 30%. As both V_1 and V_2 are smaller than the corresponding parts in the static potential by roughly the same amount, this mismatch in the Gromes identity might be due to the still incomplete cancellation of self-energy contributions in the normalization (11) of the field operator insertions. This would be a technical rather than a significant physical problem.

4. Summary

This QCD calculation, including quark-loop effects, gives clear support to the notion of scalar confinement between quarks and antiquarks. While the spin-orbit potential V_1 is of long-range character, the spin-orbit term V_2 , the tensor force V_3 and the spin-spin force V_4 are short-range as expected from the one-gluon exchange mechanism. This conforms with experimental analyses of charmonium and bottomium spectroscopy.

References

- [1] W. Buchmüller and S. Cooper, in High Energy Electron-Positron Physics, eds. A. Ali and P. Söding, World Scientific, Singapore 1989.
- [2] J.H. Kühn and P.M. Zerwas, Phys. Rep. C 167 (1988) 321.
- [3] M.J. Strassler and M.E. Peskin, Phys. Rev. D 43 (1991) 1500.
- [4] K.D. Born, E. Laermann, R. Sommer, T.F. Walsh and P.M. Zerwas, Phys. Lett. B 329 (1994) 325.
- [5] E. Eichten and F.L. Feinberg, Phys. Rev. D 23 (1981) 2724.
- [6] D. Gromes, Z. Phys. C 26 (1984) 401.
- [7] W. Lucha, F. Schöberl and D. Gromes, Phys. Rep. C 200 (1991) 127.
- [8] A.B. Henriques, B.H. Kellett and R.G. Moorhouse, Phys. Lett. B 64 (1976) 85; W. Buchmüller, Phys. Lett. B 112 (1982) 479.
- [9] M. Camprostrini, Nucl. Phys. B 256 (1985) 717; C. Michael and P.E.L. Rakow, Nucl. Phys. B 256 (1985) 640; P. de Forcrand and J.D. Stack, Phys. Rev. Lett. 55 (1985) 1254; M. Camprostrini, K. Moriarty and C. Rebbi, Phys. Rev. Lett. 57 (1986) 44; C. Michael, Phys. Rev. Lett. 56 (1986) 1219; I.J. Ford, J. Phys. G 15 (1989) 1571.
- [10] A. Huntley and C. Michael, Nucl. Phys. B 270 (1986) 123.
- [11] Y. Koike, Phys. Lett. B 216 (1989) 184.
- [12] A.M. Polyakov, Nucl. Phys. B 164 (1980) 171; V.S. Dotsenko and S.N. Vergeles, Nucl. Phys. B 169 (1980) 527.
- [13] L. Maiani, G. Martinelli and C.T. Sachrajda, Nucl. Phys. B 368 (1992) 281.
- [14] M. Albanese et al., (APE Collaboration), Phys. Lett. B 192 (1987) 163.
- [15] R. Altmeyer et al., (MT_C Collaboration), Nucl. Phys. B 389 (1993) 445.
- [16] M. Lüscher, K. Symanzik and P. Weisz, Nucl. Phys. B 173 (1980) 365.